Discovery of a cool brown dwarf

T. Nakajima*, B. R. Oppenheimer*, S. R. Kulkarni*, D. A. Golimowski†, K. Matthews* & S. T. Durrance†

* Palomar Observatory 105-24, California Institute of Technology, Pasadena, California 91125, USA
† Department of Physics and Astronomy, The Johns Hopkins University, Baltimore, Maryland 21218, USA

BROWN dwarfs are star-like objects with masses less than 0.08 times that of the Sun, which are unable to sustain hydrogen fusion in their interiors[1–4]. They are very hard to detect, as most of the energy of gravitational contraction is radiated away within $\sim 10^8$ yr, leaving only a very low residual luminosity. Accordingly, almost all searches for brown dwarfs have been directed towards clusters of young stars—a strategy that has recently proved successful[5,6]. But there are only modest observable differences between young brown dwarfs and very low-mass stars, making it difficult to identify the former without appealing to sophisticated models[7]. Older brown dwarfs should have a more distinctive appearance, and if they are companions to nearby stars, their luminosity can be determined unambiguously. Here we report the discovery of a probable companion to the nearby star Gl229, with no more than one-tenth the luminosity of the least luminous hydrogen-burning star. We conclude that the companion, Gl229B, is a brown dwarf with a temperature of less than 1,200 K, and a mass ~20–50 times that of Jupiter.

Three years ago, we initiated a search[8] for brown-dwarf companions to stars less than 15 pc away. With this strategy, we utilize the precisely known distances to these stars to determine accurately the total luminosity of any discovered companions. In all models of low-mass stars[4], the lowest luminosity of any hydrogen-burning star is $L_{min} \gtrsim 10^{-4} L_{\odot}$. Brown dwarfs of age 10^9 yr have luminosities well below L_{min} and are therefore clearly distinguishable[3] from low-mass stars. Consequently, we have begun the 'Palomar-Byr' survey, a survey of all nearby stars with ages of about one billion (10^9) years. These stars have either small space motion[9] or have active coronae (as inferred from copious Hα[10] or X-ray emission[11]), both of which are indicators of stellar youth. The survey consists of both optical coronagraphic imaging and infrared direct imaging of the stars.

During the past year, we have observed about 100 stars of this sample. Preliminary analysis of the data revealed a very intriguing proper-motion companion to the nearby star, Gl229 (also known as HD42581 and LHS1827; spectral type MlV; $M_V = 9.3$, parallax[9] 0.1749 ± 0.0045 arcsec or a distance of 5.7 pc; see ref. 12 for further details). This star was selected from a list of stars with known low space motion[9]. Based on its kinematics it has been classified as a 'young' disk star, age $\sim 10^9$ yr. However, the star exhibits Hα absorption with an equivalent width of 0.5 Å (G. Basri, J. Gizis and N. Reid, personal communication). All of the Ml stars in the Pleiades (age $\sim 10^8$ yr) show Hα in emission. However, some stars with $M_V > 9.5$ in the Hyades[13] (age $\sim 8 \times 10^8$ yr) show Hα absorption even as strongly as Gl229. This suggests that Gl229 is possibly at least as old as the Hyades. The kinematics make it unlikely that the object is older than the Sun.

We observed Gl229 with the Johns Hopkins University's Adaptive Optics Coronagraph[14] at the Cassegrain focus of the Palomar 60-inch telescope on the nights of 27 and 29 October 1994 UT. A compact source, hereafter Gl229B, was detected 7.78 ± 0.1 arcsec from Gl229 at a southeasterly position angle $PA = 163° \pm 1°$. Here PA is measured from north to east (Fig. 1). Exposures in three different bandpasses, Thuan–Gunn *r*, *i* and *z*, showed that the object was very red (Fig. 2). Infrared data of Gl229B in the J, H, K_s and K bandpasses were obtained at the Hale 200-inch telescope on the nights of 14 and 15 September 1995 UT. During October 3–8 1995 UT, Gl229 was observed again with the Adaptive Optics Coronagraph (AOC) at the Palomar 60-inch telescope. During this run, we also observed the field centred on the star θ_1 Orionis. This field has a number of stars with well determined positions[15] with respect to θ_1 Ori. These observations enabled us to derive the pixel scale (0.118 arcsec per pixel) and also determine the orientation of the CCD (charge-coupled device) detector attached to the AOC. The orientation was as expected: the CCD columns were oriented north–south to within 0.1°.

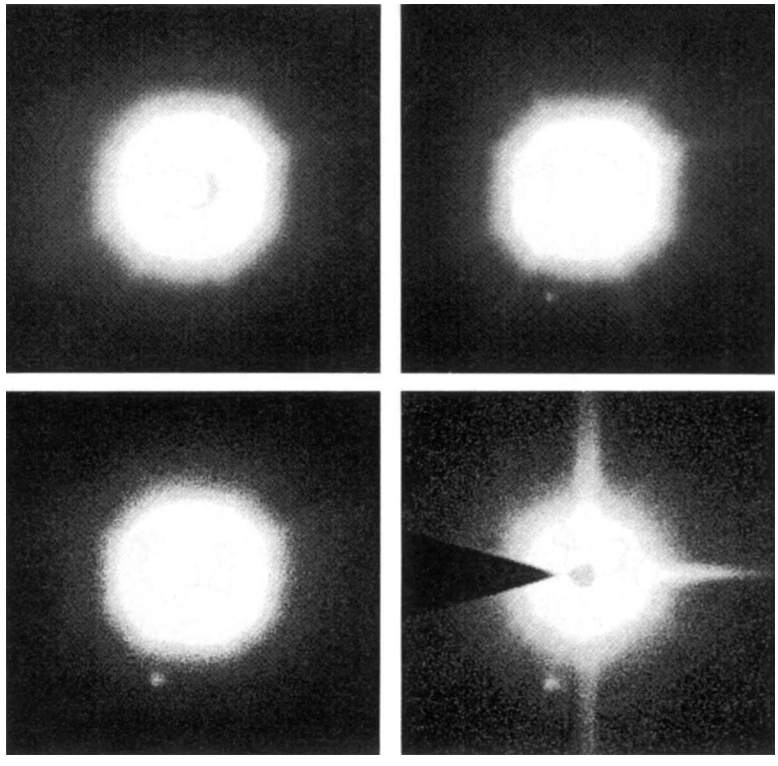

FIG. 1 Optical and infrared images of Gl229. Each field of view is 25″ × 25″, with north up and east to the left. Top left, *r*-band image; top right, *i*-band image, bottom left, *z*-band image; bottom right, K_s-band image. The logarithm of the data is displayed in all four panels. The brown-dwarf companion Gl229B is located 7.6 arcsec to the SSE of Gl229A. The *r*, *i* and *z* images were obtained on epoch 1994.82 with the Adaptive Optics Coronagraph (AOC) and the Palomar 60-inch telescope. The AOC[14] contains an image stabilizer for improved resolution and a pupil apodizer for suppression of light diffracted by the telescope aperture. The K_s image was obtained on epoch 1995.70 at the Hale 200-inch telescope. The infrared camera, located at the *f*/70 Cassegrain focus, contains reimaging optics and a Santa Barbara Research Corporation InSb detector. The secondary mirror used signals from a nearby field star to reduce image wander. A cryogenically cooled occulting disk masked Gl229A. The triangular support for this disk is seen at the left of the K_s image.

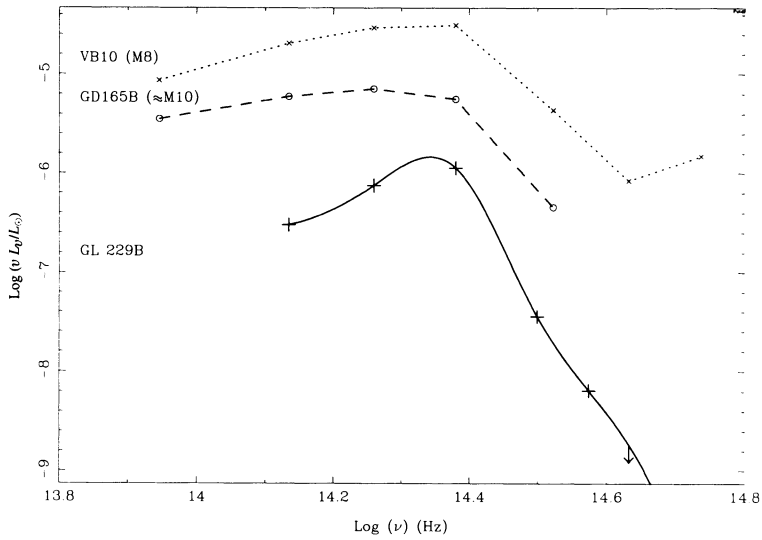

FIG. 2 Broad-band spectra of Gl229B, GD165B and VB10. The ordinate is the logarithm of νL_ν in units of solar luminosity where ν is the frequency and L_ν the luminosity per unit frequency. The spectral band in which most of the energy emerges is best indicated by this quantity. The observed magnitudes of Gl229B are $r > 22.1$ (a 10σ upper limit), $i = 20.0 \pm 0.2$, $z = 17.8 \pm 0.3$, $J = 13.5 \pm 0.1$, $H = 13.2 \pm 0.1$, $K = 13.4 \pm 0.1$ and $K_s = 13.3 \pm 0.1$. The absolute magnitudes are; $M_r > 23.3$, $M_i = 21.2 \pm 0.2$, $M_z = 19.0 \pm 0.3$, $M_J = 14.7 \pm 0.1$, $M_H = 14.4 \pm 0.1$, $M_{K_s} = 14.5 \pm 0.1$, $M_K = 14.6 \pm 0.1$, with a distance modulus of $(M - m) = +1.21 \pm 0.05$. The solid line is a cubic spline interpolation of the observed points with an extension to infinite frequency. The data for GD165B and the late M dwarf, VB10, are obtained from ref. 22. Gl229B is remarkable for both its low luminosity and its peaked spectral energy distribution.

The infrared image (Fig. 1) showed an object at the position of Gl229B. The *r*-band AOC images contain six stars, excluding Gl229, spread over the field of view of 1 arcmin^2. We compared the relative positions of these stars in the 1994 and 1995 images. We found that there was very little change in the pixel scale, but that the 1994 image was rotated $1.8° \pm 0.2°$ with respect to the 1995 image. This comparison also yielded an empirical measure of the root-mean-square error, $\sigma \sim 1$ pixel in each axis, in the fiducial centre of the star (centroid). The occulting disk had enough transmission that we could satisfactorily centre on Gl229. From 1994 to 1995, we found that Gl229 had moved, with respect to the six field stars, by 0.3 ± 1 pixel to the west and 4.5 ± 1 pixel to the south. This is consistent with the known proper motion[12] of Gl229, 0.737 arcsec yr^{-1} and PA = 190.2°. Gl229B is not detected in the *r*-band AOC image but is easily detected in the *z*-band image. Unfortunately, only two of the six field stars are seen in this image. With respect to these, Gl229B had moved 0 ± 1.5 pixel to the west and 3.7 ± 1.5 pixel to the south. Thus within the errors, it appears that Gl229B is a common proper-motion companion of Gl229. It is appropriate to refer to Gl229 as Gl229A.

Our argument of companionship is based on two measurements, obtained about one year apart. It is certain that Gl229B is not a distant object because it has a measurable proper motion. It is conceivable, though improbable, that Gl229B is a foreground object, unrelated to Gl229A. Fortunately, this issue can be resolved through observations. Specifically, measurement of the parallax (easily possible with the Hubble Space Telescope) of Gl229B is the most definitive way to confirm companionship.

To undertake further observations (for example, long-slit spectroscopy) it is necessary to obtain the precise offset of Gl229B with respect to Gl229A. This is best done using the infrared data rather than the AOC data for the following reason. At optical wavelengths, the contrast (C) defined as the ratio of the brightness of Gl229A to Gl229B is extremely large (wavelength $\lambda \sim 0.65$ μm, $C > 10^6$; $\lambda \approx 0.80$ μm, $C = 4 \times 10^5$; $\lambda \approx 0.9$ μm, $C \approx 8 \times 10^4$). For this reason, we have to use a coronagraph in order to image Gl229B and Gl229A simultaneously. However, spatial variations in the transparency across the occulting disk will bias the determination of the centroid of Gl229A but not that of Gl229B. An additional complication is the point-spread function varies across the field of view of the coronagraph. The situation is far more favourable at infrared wavelengths where $C \approx 60$ and thus direct imaging techniques can be used. From a number of short and long exposures we find that Gl229B is located 7.69 ± 0.1 arcsec from Gl229A at PA = $162° \pm 1°$. The pixel scale and the orientation of the infrared camera are extremely well determined and known to be very stable.

The magnitudes of Gl229B are given in Fig. 2. The total (or bolometric) luminosity L can be obtained by integrating the broad-band spectrum shown in Fig. 2. This integration yields $L \approx 2 \times 10^{-6} L_\odot$. It is possible that there is considerable emission at frequencies smaller than the lowest measured frequency at K band. However, this method overestimates the total emission due to the presence of opacity between the observed bands. For these reasons, an accurate estimation of the total emission requires guidance from models of brown-dwarf atmospheres. These models are still in their infancy, and they critically rely on effective temperature, $T_{\rm eff} = (L/4\pi R^2 \sigma)^{1/4}$, where R is the radius and σ is the Stefan–Boltzmann constant. For brown dwarfs[3,4], $R \approx 0.1 R_\odot$. We obtain $T_{\rm eff} = 700$ K for Gl229B. Only the models of Tsuji *et al.*[16] are applicable to such a low $T_{\rm eff}$. They predict $K - L' = 2$ for the observed $J - K = 0.15$ and $T_{\rm eff} \approx 1{,}000$ K. Incorporating the predicted L' and extrapolating the low-frequency tail with a Rayleigh–Jeans formula, we obtain $L \approx 4 \times 10^{-6} L_\odot$.

The definition of a brown dwarf depends on its mass being less than 80 times the mass of Jupiter. However, with the data at hand, it is not possible to determine the mass of Gl229B from dynamical considerations[17]. But according to models of low-mass stars[4], the luminosity of the lowest-mass star is $L_{\rm min} \gtrsim 10^{-4} L_\odot$. This is about equal to the luminosity[18,19] of GD165B. Unfortunately, the mass of this object is unknown. It is certainly on the threshold of the star–substellar boundary. The red dwarf with the lowest determined dynamical mass[17] is GJ1245C, $M = 0.074 \pm 0.013 M_\odot$. The luminosity of this star is $\sim 5 \times 10^{-4} L_\odot$. For Gl229B, we make the conservative assumption of $L < 10^{-5} L_\odot$ which is more than order of magnitude smaller than the luminosity of either of these two objects. Thus we conclude that Gl229B is certainly a brown dwarf. Below we argue that the peculiar broad-band spectrum of Gl229B constitutes an independent line of reasoning that supports this conclusion.

We now use brown-dwarf cooling models to estimate the mass of Gl229B. According to these models[4], the luminosity of a brown dwarf older than 10^8 yr is

$$L = 3.4 \times 10^{-6} L_\odot t_9^{-1.3} (M/20 M_J)^{2.64}$$

where t_9 is the age of the brown dwarf in billions of years, M is the mass of the brown dwarf, and M_J is the mass of Jupiter. Thus we infer a mass of $\sim 20\sqrt{t_9} M_J$. Earlier we argued that t_9 is of the order of unity. Even if t_9 is as high as 6, the estimated mass is still below the maximum mass for brown

dwarfs. All this discussion assumes that Gl229A and Gl229B are coeval.

The broad-band spectrum of Gl229B is unlike that of any known star or for that matter any known celestial object. Specifically, the infrared colour is blue whereas the optical colour is extremely red (Fig. 2). The spectral energy distribution peaks at J band, $\lambda \approx 1.25$ μm. This is indeed predicted by recent models of brown-dwarf atmospheres[16,20]. This phenomenon is reproduced by all models regardless of the details of the input molecular opacities. At high pressures and low temperatures, characteristic of atmospheres of brown dwarfs, H_2O and CH_4 are formed abundantly and these molecules essentially limit the transmission to the near-infrared band of 1.2 μm. The cool temperature results in very little emission below 1 μm. These two effects conspire to produce a peak at J band. Thus we argue that the peculiar broad-band spectrum provides additional evidence that Gl229B is a cool brown dwarf. Elsewhere[21] we report the detection of strong methane absorption in the spectrum of this object which provides the definitive proof that Gl229B is a cool object, $T_{\rm eff} < 1{,}200$ K.

We end with some suggestions and speculations. First, searches for isolated brown dwarfs should take advantage of the peculiar colours such as those we see in Gl229B. Specifically, the searches should not use infrared colours alone as a discriminant, but rather compare optical flux to any infrared flux. Second, the projected separation of Gl229B is 44 astronomical units, which is about the distance from the Sun to Pluto. Thus the orbital motion of Gl229B should be 0.1 arcsec yr^{-1}. Observations with the Hubble Space Telescope could easily measure this. Newly commissioned infrared interferometers have sufficient precision that the mass of Gl229B could be determined over the next few years, provided that the orbit is circular. □

Received 25 September; accepted 13 November 1995.

1. Kumar, S. S. *Astrophys. J.* **137,** 1121–1126 (1963).
2. Tartar, J. C. in *Astrophysics of Brown Dwarfs* (eds Kafatos, M. C., Harrington, R. S. & Maran, S. P.) 121–138 (Cambridge Univ. Press, 1986).
3. Stevenson, D. J. *A. Rev. Astr. Astrophys.* **29,** 163–193 (1991).
4. Burrows, A. & Liebert, J. *Rev. mod. Phys.* **65,** 301–336 (1993).
5. Basri, G., Marcy, G. W. & Graham, J. R. *Astrophys. J.* (in the press).
6. Rebolo, R., Zapatero Osorio, M. R. & Martin, E. L. *Nature* **377,** 129–131 (1995).
7. Magazzù, A., Martin, E. L. & Rebolo, R. *Astrophys. J.* **404,** L17–L20 (1993).
8. Nakajima, T., Durrance, S. T., Golimowski, D. A. & Kulkarni, S. R. *Astrophys. J.* **428,** 797–804 (1994).
9. Leggett, S. K. *Astrophys. J. Suppl. Ser.* **82,** 351–394 (1992).
10. Hawley, S. L. in *The Bottom of the Main Sequence—and Beyond* (ed. Tinney, C. G.) 224–227 (Springer, Berlin, 1995).
11. Pallavicini, R. *Astr. Astrophys. Rev.* **1,** 177–207 (1989).
12. Gliese, W. & Jahreiss, H. *Preliminary Version of the Third Catalog of Nearby Stars* (1991).
13. Reid, I. N., Hawley, S. L. & Mateo, M. *Mon. Not. R. astr. Soc.* **272,** 828–842 (1995).
14. Golimowski, D. A., Clampin, M., Durrance, S. T. & Barkhouser, R. H. *Appl. Opt.* **31,** 4405–4416 (1992).
15. Hirschfeld, A. & Sinnott, R. W. *Sky Catalog 2000.0* Vol. 2 (Cambridge Univ. Press, Sky Publishing, Cambridge, 1995).
16. Tsuji, T., Ohnaka, K. & Aoki, W. in *The Bottom of the Main Sequence—and Beyond* (ed. Tinney, C. G.) 45–49 (Springer, Berlin, 1995).
17. Henry, T. J. & McCarthy, D. W. *Astr. J.* **106,** 773–789 (1993).
18. Zuckerman, B. & Becklin, E. E. *Astrophys. J.* **386,** 260–264 (1992).
19. Tinney, C. G., Mould, J. R. & Reid, I. N. *Astr. J.* **105,** 1045–1059 (1993).
20. Allard, F. & Hauschildt, H. P. in *The Bottom of the Main Sequence—and Beyond* (ed. Tinney, C. G.) 32–40 (Springer, Berlin, 1995).
21. Oppenheimer, B. R., Kulkarni, S. R., Matthews, K. & Nakajima, T. *Science* (in the press).
22. Jones, H. R. A., Longmore, A. J., Jameson, R. F. & Mountain, C. M. *Mon. Not. R. astr. Soc.* **267,** 413–423 (1994).

ACKNOWLEDGEMENTS. We thank P. Goldreich, E. S. Phinney, I. N. Reid and M. van Kerkwijk for discussions. Some of the observations were conducted at the Palomar 60-inch telescope, which is jointly owned by the California Institute of Technology and the Carnegie Institution of Washington. At Caltech, this research was initiated from a seed grant from the Flintridge Foundation. S.R.K. is deeply indebted to the Foundation. The construction of the AOC was funded by the Seaver Institute. S.T.D. is grateful for their generous support. Our current activities are supported by the Packard Foundation, the US NSF and NASA. Infrared astronomy at Palomar is supported by the US NSF. B.R.O. is supported by an NSF graduate Fellowship. D.A.G. and S.T.D. thank the Center for Astrophysical Sciences at JHU for its support of this work.

Taming spatiotemporal chaos with disorder

Y. Braiman*†, John F. Lindner*‡ & William L. Ditto*

* Applied Chaos Laboratory, School of Physics, Georgia Institute of Technology, Atlanta, Georgia 30332, USA
‡ The College of Wooster, Wooster, Ohio 44691, USA

Disorder and noise in physical systems usually tend to destroy spatial and temporal regularity, but recent research into nonlinear systems provides intriguing counter-examples. In the phenomenon of stochastic resonance[1], for example, the presence of noise improves the ability of some nonlinear systems to transfer information reliably. Noise can also remove chaos in a model oscillator[2], and facilitate synchronization in an extended array of bistable elements[3]. Here we explore the use of disorder as a means to control spatiotemporal chaos[4–8] in coupled arrays of forced, damped, nonlinear oscillators. Chaotic behaviour in spatially extended systems, especially in biology and physiology[9,10], might be amenable to control, as occurs in low-dimensional temporally chaotic systems[11,12]. In our numerical experiments, one- and two-dimensional arrays of identical oscillators behave chaotically, but the introduction of slight, uncorrelated differences between the oscillators induces ordered motion characterized by complex but regular spatiotemporal patterns.

If our oscillators are identical, then our arrays are chaotic. (Nearby trajectories in the phase space of the array diverge exponentially, as measured by a positive Lyapunov exponent). Making the oscillators non-identical by introducing disorder into a parameter that characterizes their behaviour, removes the chaos and freezes-in complex spatiotemporal patterns by frequency-locking the motion to harmonics and subharmonics of the forcing. (Frequency-locking is distinct from phase-locking: the former tames chaos whereas the latter need not, as a synchronized array may be chaotic.) This phenomenon appears robust with respect to both the parameter range and the size and realization of the disorder. In fact, when we numerically calculate the leading Lyapunov exponent of the array as a function of the size of the disorder, we find large regions in parameter space where disorder leads to complete frequency-synchronization of the array. Moreover, we have observed this effect in multiple systems.

To demonstrate the phenomenon clearly, we first suggest an intentionally simple example. We consider a one-dimensional array (or chain) of forced, damped, nonlinear pendula governed by the equation

$$ml_n^2\ddot{\theta}_n + \gamma\dot{\theta}_n = -mgl_n \sin\theta_n + \tau' + \tau \sin\omega t + \kappa(\theta_{n+1} - \theta_n) + \kappa(\theta_{n-1} - \theta_n)$$

where $n = 1, 2, \ldots, N$, and where the ends are free ($\theta_0 = \theta_1$ and $\theta_N = \theta_{N+1}$). For simplicity, we take the acceleration due to gravity $g = 1.0$ and the mass of the pendulum bob $m = 1.0$. Other parameters are damping $\gamma = 0.75$, length $l_n = 1.0$, d.c. torque $\tau' = 0.7155$, a.c. torque $\tau = 0.4$, angular frequency $\omega = 0.25$, coupling $\kappa = 0.5$. We numerically integrate the equations of motion using a fourth-order Runge–Kutta technique with a time step $dt = T/2{,}500$, where $T = 2\pi/\omega$.

Each isolated (uncoupled) pendulum operates in a region of parameter space consisting of a region of chaotic orbits separating regions of qualitatively distinct periodic orbits. The default length $l = 1.0$ results in chaotic motion, characterized by a posi-

† Present address: School of Physics, Emory University, Atlanta, Georgia 30322, USA.